Design of Customized Adaptive Radar Detectors in the CFAR Feature Plane

Angelo Coluccia, *Senior Member, IEEE*, Alessio Fascista, *Member, IEEE*, and Giuseppe Ricci, *Senior Member, IEEE*

***Abstract*—The paper addresses the design of adaptive radar detectors with desired behavior, in Gaussian disturbance with unknown statistics. Specifically, based on detection probability specifications for chosen signal-to-noise ratios and steering vector mismatch levels, a methodology for the design of customized constant false alarm rate (CFAR) detectors is devised in a suitable feature plane obtained from two maximal invariant statistics. To overcome the analytical and numerical intractability of the resulting optimization problem, a novel general reduced-complexity algorithm is developed, which is shown to be effective in providing a feasible solution (i.e., fulfilling a constraint on the probability of false alarm) while controlling the behavior under both matched and mismatched conditions, so enabling the design of fully customized adaptive CFAR detectors.**

***Index Terms*—Radar, GLRT, CFAR property, robust detectors, selective detectors, mismatched signals, feature space.**

I. Introduction

THE detection of targets embedded in Gaussian disturbance composed of thermal noise, clutter, and possible jamming interferers is a central problem in the radar detection literature. A consolidated approach is to resort to the generalized likelihood ratio test (GLRT) approach, in which the statistics of the disturbance are estimated through the aid of a set of secondary data, having the same statistics as H_0. Since the pioneering work by Brennan and Reed [1], and then Kelly [2], particular focus has been put on obtaining statistics that do not depend upon unknown clutter or noise statistics under the H_0 hypothesis: this in fact guarantees that the detection threshold can be set to ensure a prefixed false alarm probability (P_{fa}), a property referred to as constant false alarm rate (CFAR).

Several adaptive detectors have been derived in the past decades based on such a rationale [3], [4]. Significant attention has been paid to the design of CFAR detectors with desired properties in terms of probability of detection (P_d) under mismatched conditions. Typically, a robust detector is desirable to cope with possible off-grid conditions due to angle and/or Doppler quantization, which imply that the actual steering vector may be not aligned with the nominal one; conversely, a selective detector is desirable to reject unwanted signals due to jamming or spectrum co-existence [5]. In this respect, Kelly's detector is a moderately selective receiver [6], while the adaptive matched filter (AMF) [7] is a robust receiver. Other well-known examples of selective receivers are the adaptive coherence estimator (ACE) [8] (also called adaptive normalized matched filter), the ABORT or whitened-ABORT (WABORT) detectors [9], [10], [11], as well as the Rao detector [12]. A further type of receivers is based on the idea of inserting a parameter in a well-known statistic, so as to obtain a tunable detector: for instance, in Kalson's detector [13] a nonnegative parameter is introduced in the Kelly's statistic, in order to control the rejection level of mismatched signals, in between the AMF and Kelly's detector.

The design of detectors with suitable symmetries that can also ensure the CFAR behavior has found an important theoretical tool in the principle of invariance [14], [15], [16], [17]. In our previous work [18], a "CFAR feature plane" (CFAR-FP) is introduced for a suitable maximal invariant of the classical adaptive radar detection problem after Kelly's formulation. In the CFAR-FP, radar returns are mapped to two-dimensional clusters whose properties in terms of position and shape in the plane can be analytically characterized and expressed as a function of few main parameters, so shedding new light on the behavior of several well-known CFAR detectors.

The use of the invariance principle and maximal invariant statistics as key elements in the design of adaptive radar detectors has been an active research field in the last years. Invariance theory turned out to be useful in heterogeneous environments, characterized by Gaussian interference with spatially varying power, to derive a class of detection rules exhibiting specific symmetries that ensure the CFAR property [19]. In [20], detection of targets embedded in Gaussian disturbance sharing a block-diagonal covariance structure is addressed. A unified framework considering point-like, range-spread, and subspace targets is provided to model the general problem, and a new family of invariant detectors is proposed to overcome the unavailability of the GLRT in closed-form. In [21], authors dealt with the problem of target detection in (possibly low-rank) dominant heterogeneous clutter plus Gaussian thermal noise. Two tunable invariant detectors derived from equivalent binary hypothesis tests with observations having block-diagonal covariance matrices are proposed, which guarantee bounded CFAR property.

One of the challenges in adaptive coherent detection is how to ensure a prefixed P_{fa} and, at the same time, control the behavior under both matched and mismatched conditions, while guaranteeing the CFAR property (as better discussed in Section II). Moreover, enhancing either the robustness or the selectivity of a radar detector often comes at the price of a P_d loss under matched conditions [22]. Although [18] provided tools for interpreting the

Manuscript received 8 April 2022; revised 18 August 2022 and 13 October 2022; accepted 14 October 2022. Date of publication 21 October 2022; date of current version 7 November 2022. The associate editor coordinating the review of this manuscript and approving it for publication was Dr. Bo Tang. *(Corresponding author: Angelo Coluccia.)*

The authors are with the Dipartimento di Ingegneria dell'Innovazione, Università del Salento, 73100 Lecce, Italy (e-mail: angelo.coluccia@unisalento.it; alessio.fascista@unisalento.it; giuseppe.ricci@unisalento.it).

Digital Object Identifier 10.1109/TSP.2022.3216372

performance of CFAR detectors, the design therein was mostly heuristic. Indeed, the development of a general methodology for the design of fully customized adaptive CFAR detectors is still an open research problem.

Aiming at advancing the literature towards this direction, in the present paper an original design methodology is devised based on the CFAR-FP. Specifically, after introducing the required background and discussing in detail the importance of having an analytical framework to guide the design of customized detectors in the CFAR-FP in Section II, the following contributions are provided:

- Given P_d specifications for chosen numerical values of signal-to-noise ratios and steering vector mismatch levels (examples are discussed in Section III-A), corresponding to a desired detection behavior, the optimal infinite-dimensional problem of designing a customized CFAR detector working at a preassigned P_{fa} is formulated, with suitable cost function and constraint (Section III-B). To overcome its mathematical intractability, a finite-dimensional version is considered (Section III-C), using a suitable parametric family of approximation functions. However, the resulting optimization problem is still highly-nonlinear and state-of-the-art numerical methods attempting at jointly optimizing all the involved parameters fail in providing a feasible solution satisfying the P_{fa} constraint (Section IV-A).
- To address such a challenge, a novel, low-complexity, sub-optimal search strategy in a reduced, though sufficiently rich, solution space is devised. Using a piecewise-linear structure for the approximation functions, convenient analytical formulas are derived to ease the evaluation of the cost function and provide a closed-form expression for the P_{fa} constraint (Section IV-B). Though inherently sub-optimal, the proposed algorithm represents (to the best of the authors' knowledge) the first method able to find a feasible solution (i.e., exactly fulfilling the P_{fa} constraint) to the intractable optimization problem for designing customized CFAR detectors with desired properties.
- The effectiveness of the proposed approach, which is fully general and does not depend upon the unknown statistics of the disturbance, is demonstrated by designing two novel detectors representative of either robust or selective behaviors (among the examples of Section III-A). The approximation accuracy is evaluated in comparison with a plain solution, and a performance assessment against well-known detectors is also performed (Section V). A thorough performance analysis conducted on both simulated and real-world radar measurements shows that the proposed approach is effective in providing a satisfactory approximation of the desired detector, while ensuring a prefixed P_{fa} and controlling the behavior under both matched and mismatched conditions, which is of utmost importance in radar applications.

We conclude the paper in Section VI.

In the following, vectors and matrices are denoted by boldface lower-case and upper-case letters, respectively. The (i,j)th entry of a matrix $\boldsymbol{A}$ is indicated by $[\boldsymbol{A}]_{i,j}$. Symbols $(\cdot)^{\mathsf{T}}$, $(\cdot)^{\dagger}$, and $|\cdot|$ denote the transpose, conjugate transpose, and modulus operators, respectively. The functions $F_x(\cdot)$ and $p(\cdot)$ denote the cumulative distribution function (CDF) of the random variable x and the probability density function (pdf), respectively. $\Pi(\cdot)$ is the rectangular window centered in the origin with unitary amplitude over $[-1/2, 1/2]$ (and zero elsewhere). As to numerical sets, $\mathbb{C}$ is the set of complex numbers and $\mathbb{C}^{P\times Q}$ is the Euclidean space of $(P \times Q)$-dimensional complex matrices (or vectors if $Q = 1$). $\boldsymbol{I}_{P\times Q}$ and $\boldsymbol{0}_{P\times Q}$ stand for the identity matrix and the null matrix of dimension $P \times Q$.

II. Background and Motivation

In this section we recall the classical formulation of the radar detection problem, and review its interpretation in the CFAR-FP introduced in [18]. This will serve to provide the necessary background, for self-consistency, and also to illustrate in more details the motivation of the present work.

A. Problem Formulation

The classical hypothesis testing problem for detecting the possible presence of a (point-like) coherent target from a given cell under test (CUT) is given by

$$\begin{cases} H_0: & \boldsymbol{z} = \boldsymbol{n} \\ H_1: & \boldsymbol{z} = \alpha \boldsymbol{v} + \boldsymbol{n} \end{cases} \tag{1}$$

where $\boldsymbol{z} \in \mathbb{C}^{N\times 1}$, $\boldsymbol{n} \in \mathbb{C}^{N\times 1}$, and $\boldsymbol{v} \in \mathbb{C}^{N\times 1}$ are the received vector, the overall disturbance term, and the known space-time steering vector of the target. The unknown deterministic parameter $\alpha \in \mathbb{C}$ is the target amplitude, depending on radar cross-section, multipath, and other channel effects.

Kelly [2] derived a GLRT for problem (1) assuming complex normal distributed $\boldsymbol{n}$ with zero mean and unknown (Hermitian) positive definite covariance matrix $\boldsymbol{C}$, and $K \geq N$ independent and identically distributed training (or secondary) data $\boldsymbol{z}_1, \ldots, \boldsymbol{z}_K$ (independent of $\boldsymbol{z}$, free of target echoes, and sharing with the CUT the statistical characteristics of the noise). Let $\boldsymbol{S} = \sum_{k=1}^{K} \boldsymbol{z}_k \boldsymbol{z}_k^{\dagger}$, then Kelly's statistic is

$$t_{\text{Kelly}} = \frac{|\boldsymbol{z}^{\dagger}\boldsymbol{S}^{-1}\boldsymbol{v}|^2}{\boldsymbol{v}^{\dagger}\boldsymbol{S}^{-1}\boldsymbol{v}\,(1 + \boldsymbol{z}^{\dagger}\boldsymbol{S}^{-1}\boldsymbol{z})}. \tag{2}$$

Eq. (2) can be rewritten as $t_{\text{Kelly}} = \frac{\tilde{t}}{1+\tilde{t}}$, where

$$\tilde{t} = \frac{|\boldsymbol{z}^{\dagger}\boldsymbol{S}^{-1}\boldsymbol{v}|^2}{\boldsymbol{v}^{\dagger}\boldsymbol{S}^{-1}\boldsymbol{v}\,\left(1 + \boldsymbol{z}^{\dagger}\boldsymbol{S}^{-1}\boldsymbol{z} - \frac{|\boldsymbol{z}^{\dagger}\boldsymbol{S}^{-1}\boldsymbol{v}|^2}{\boldsymbol{v}^{\dagger}\boldsymbol{S}^{-1}\boldsymbol{v}}\right)} \tag{3}$$

hence t_{Kelly} and $\tilde{t}$ are equivalent statistics (and of course $\tilde{t} = \frac{t_{\text{Kelly}}}{1-t_{\text{Kelly}}}$). As mentioned, a remarkable property of Kelly's detector is that it has the CFAR property; moreover, it behaves as a moderately selective detector when the actual steering vector $\boldsymbol{p}$ in the received signal $\boldsymbol{z}$ is not aligned with the nominal one $\boldsymbol{v}$. The mismatch level is quantified by the squared cosine of the angle between these two vectors, i.e.,

$$\cos^2\theta = \frac{\boldsymbol{p}^{\dagger}\boldsymbol{C}^{-1}\boldsymbol{v}}{\boldsymbol{p}^{\dagger}\boldsymbol{C}^{-1}\boldsymbol{p}\;\boldsymbol{v}^{\dagger}\boldsymbol{C}^{-1}\boldsymbol{v}}. \tag{4}$$

Invariance theory has shown that CFAR detectors in Gaussian disturbance can be written in terms of equivalent pairs of maximal invariant statistics; a convenient choice adopted in [18] is $(\beta, \tilde{t})$, where

$$\beta = \frac{1}{1 + \boldsymbol{z}^{\dagger}\boldsymbol{S}^{-1}\boldsymbol{z} - \frac{|\boldsymbol{z}^{\dagger}\boldsymbol{S}^{-1}\boldsymbol{v}|^2}{\boldsymbol{v}^{\dagger}\boldsymbol{S}^{-1}\boldsymbol{v}}} \in [0, 1]. \tag{5}$$

On the geometric side, this means that signals from the CUT and secondary cells are mapped, through (3) and (5), into two-dimensional points $(\beta, \tilde{t})$ of the CFAR-FP. The colored dots

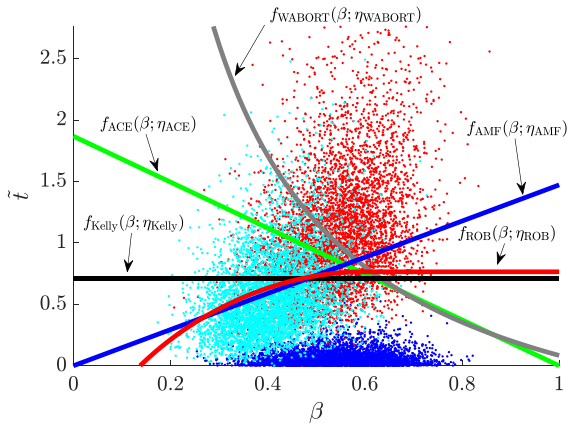

Fig. 1. Some well-known detectors in the CFAR-FP, for $N = 8$, $K = 16$, $P_{fa} = 10^{-4}$. Blue dots are the H_0 cluster, red dots are the H_1 cluster for SNR $= 15$ dB, while cyan dots represent a cluster under mismatched conditions ($\cos^2\theta = 0.65$).

shown in Fig. 1 indeed represent several realizations of the random variables $(\beta, \tilde{t})$, obtained from data vectors $\boldsymbol{z}, \boldsymbol{z}_1, \ldots, \boldsymbol{z}_K$: specifically, blue dots correspond to data under H_0 (noise only), red dots are the data under H_1 for 15 dB of signal-to-noise ratio (SNR) defined as

$$\gamma = |\alpha|^2 \boldsymbol{p}^\dagger \boldsymbol{C}^{-1} \boldsymbol{p} \in \mathbb{R}_+ \tag{6}$$

whereas cyan dots are for H_1 with the same SNR but under mismatched conditions (with $\cos^2\theta \approx 0.46$). Finally, the test associated to a generic CFAR detector X (including AMF, ACE, Kalson, etc.) can be rewritten as

$$t_X(\beta, \tilde{t}) \underset{H_0}{\overset{H_1}{\gtrless}} \eta_X \tag{7}$$

where t_X is the decision statistic and η_X is the threshold that guarantees the desired P_{fa}; its geometrical interpretation in the CFAR-FP is discussed as follows.

B. Detection in the CFAR Feature Plane

It has been shown in [18] that in most cases the curve $t_X(\beta, \tilde{t}) = \eta_X$ in the β-$\tilde{t}$ CFAR-FP can be made explicit in $\tilde{t}$ as a function of β, meaning that (7) is equivalent to

$$\tilde{t} \underset{H_0}{\overset{H_1}{\gtrless}} f_X(\beta; \eta_X) \tag{8}$$

where f_X is called *decision region boundary* and separates the plane in two regions: for data points falling in the bottom-most part the detector will decide for H_0, while for the upper-most part it will decide for H_1, as shown in Fig. 1. For instance, Kelly's detector is a very special case of (8) with a constant decision region boundary $f_{\text{Kelly}}(\beta; \eta_{\text{Kelly}}) = \eta_{\text{Kelly}}$. Similarly, the AMF has a linear decision region boundary $f_{\text{AMF}}(\beta; \eta_{\text{AMF}}) = \beta\eta_{\text{AMF}}$ and likewise for the ACE we have $f_{\text{ACE}}(\beta; \eta_{\text{ACE}}) = -\frac{\eta_{\text{ACE}}}{1-\eta_{\text{ACE}}}\beta + \frac{\eta_{\text{ACE}}}{1-\eta_{\text{ACE}}}$. More examples of linear and non-linear decision region boundaries are provided in Table I of [18].

Several insights on the detection behavior were obtained in [18] by studying how such decision region boundaries relate, as shown in Fig. 1, to the clusters of data points $(\beta, \tilde{t})$ which concentrate or spread according to the mismatch level $\cos^2\theta$ (given in (4)) and SNR (given in (6)). In particular, Kelly's horizontal boundary $f_{\text{Kelly}}(\beta; \eta_{\text{Kelly}})$ best separates the H_0 cluster from any H_1 cluster under matched conditions; conversely, detectors with robust/selective behaviors exhibit oblique linear/non-linear boundary, with increasing trend for robust behavior and decreasing trend for selective behavior, as visible in Fig. 1, respectively, for AMF and the robustified GLRT (ROB) [23] and for ACE and WABORT. The ROB in particular has P_d similar to Kelly's detector under matched conditions but is very robust: in fact, its decision region boundary $f_{\text{ROB}}(\beta; \eta_{\text{ROB}})$ is increasing in the lower range of β, as the AMF, and then becomes constant (horizontal) for larger values, as Kelly's detector, so combining the characteristics of both detectors. Another decision scheme that combines the characteristics of two well-known detectors naturally arises when a K-nearest neighbors decision rule is adopted, resulting in an intermediate behavior (as well as decision region boundary) between Kelly's detector and AMF [24], [25].

C. Design Challenges and Motivations

Unfortunately, a general methodology for the design of customized detectors (including, but not limited to, combinations of two or more existing detectors) with prescribed behavior in terms of P_d under matched and mismatched conditions is still missing in the literature. In the CFAR-FP, this corresponds to choosing an arbitrary decision region boundary of interest, denoted as $d(\beta)$, according to the intended classification of signal points for different SNRs and mismatch levels (clusters) as either H_0 or H_1. However, the P_{fa} of the resulting detector

$$\tilde{t} \underset{H_0}{\overset{H_1}{\gtrless}} d(\beta)$$

cannot be controlled upfront, not even when joining parts taken from existing detectors having common P_{fa}. Indeed, the relationships between decision region boundary and the induced P_{fa} and P_d's (under matched and mismatched conditions) are highly non-linear, as discussed in [18] and recalled later in this paper; thus, any adjustment around a certain region of the curve (aimed at matching the P_{fa}) will have an uneven impact according to the density of points (belonging to the different clusters) that fall in that region of the CFAR-FP — so making such an adjustment unintuitive and non-trivial. The naive solution adopted in [18] to adjust the P_{fa} was to stiffly shift the desired curve $d(\beta)$ upwards or downwards, iteratively, while checking P_{fa} and stopping at equality. As it can be seen from Fig. 2, if for instance $d(\beta)$ (dashed line) yields a P_{fa} higher than the chosen value ψ — meaning that the integral of the joint pdf of $(\beta, \tilde{t})$ over the area above the curve exceeds ψ — the curve is shifted upwards. This will result in a decrease of P_{fa} since less points of the H_0 cluster will fall above the decision boundary of the shifted $d(\beta)$. The process is iterated, by shifting the curve upwards or downwards according to the computed value of P_{fa}, until the exact shift is found for which the corresponding P_{fa} perfectly matches ψ (shown with solid line in Fig. 2). Unfortunately, in doing so the performance in terms of P_d and/or desired behavior under mismatched conditions will be affected, i.e., the shift may generally jeopardize the design.

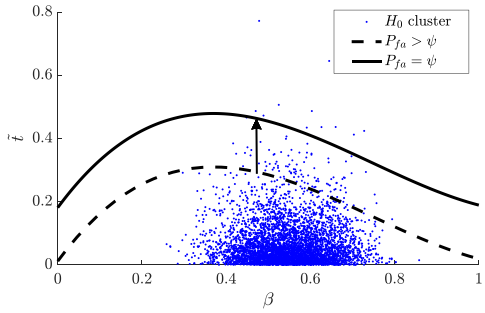

Fig. 2. Adjustment of P_{fa} by stiff shift of a decision region boundary.

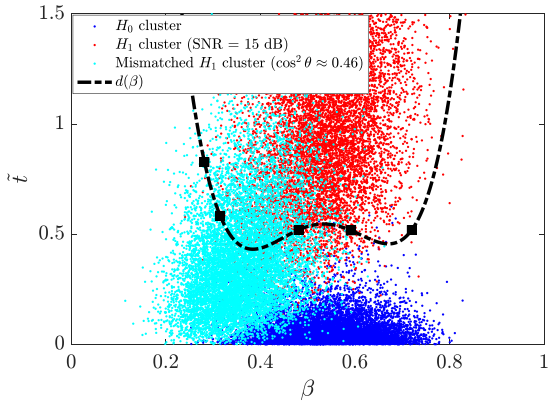

Fig. 3. Desired decision region boundary $d(\beta)$ of the double-well detector in the CFAR-FP.

The discussion above motivates the importance of addressing the design of customized detectors in the CFAR-FP under a formal optimization framework, for any given $d(\beta)$, while guaranteeing a preassigned P_{fa}, as discussed below.

III. Proposed Design of Customized Adaptive CFAR Radar Detectors

A. Preliminary Considerations and Design Examples

Considering the goal of designing customized detectors with desired properties that work at a preassigned P_{fa}, the starting point is the decision region boundary $d(\beta)$ of a desired CFAR detector. It is irrelevant how such an expression is obtained: the most general case consists in directly drawing $d(\beta)$ in the CFAR-FP according to an intended classification of signal points as either H_0 or H_1. In Fig. 3 we report, as a first example, a possible customized detector aimed at exhibiting good rejection capabilities of mismatched signals while providing high P_d under matched conditions; given its shape, it will be referred to as "double-well" detector. The desired $d(\beta)$ is obtained as a fourth-order spline parameterized by five control points, thus interpolating them: the first two are chosen in correspondence of the upper left-most part of the mismatched H_1 cluster, while the remaining three are set to better separate the matched H_1 cluster from H_0 according to the points dispersion, without including too many points of the mismatched H_1 cluster that fall underneath $d(\beta)$.

Alternatively, special cases of $d(\beta)$ can be obtained by combining two or more decision region boundaries of well-known detectors for non-overlapping intervals of β, as discussed in Section II, according to the desired performance. A possibility

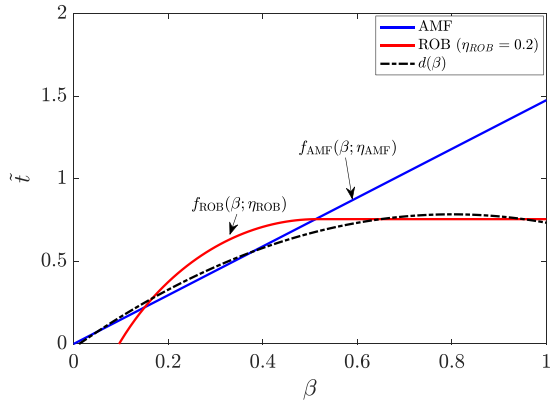

Fig. 4. Desired decision region boundary $d(\beta)$ obtained as a combination of ROB and AMF detectors.

is to take selected points from the curves of different existing detectors over the domain $\beta \in [0, 1]$, and use them as control points for fitting a (low-order) spline; this will result in a curve with "intermediate" characteristics (not necessarily passing through all control points). An example is shown in Fig. 4, where the AMF and ROB detectors have been selected and a third-order spline has been used for the fitting. Clearly, it is also possible to simply juxtapose the parts taken from the different detectors, without any interpolation.

The central problem addressed in the paper is thus how to obtain an implementable detector that is "close" to the chosen $d(\beta)$ but at the same time fulfills a given P_{fa} constraint. The latter is indeed not generally satisfied by an arbitrary choice of $d(\beta)$, neither when it is inspired to existing CFAR detectors (even when they work, individually, at the desired P_{fa}) nor when it is chosen based on the locations and spread of the H_0 and H_1 data clusters.

B. Infinite-Dimensional Design Problem

We recall that $d(\beta)$ is a CFAR detector selected by the designer for its desired performance under matched and mismatched conditions. However, as anticipated, the resulting value of P_{fa} is unpredictable, even in case of combination of detectors with the same P_{fa}. In order to come up with a detector working at a preassigned P_{fa}, which is of fundamental importance in the radar context, a strategy is needed that starts from $d(\beta)$ and approximates it through a suitable parametric function until the P_{fa} constraint is exactly fulfilled, while retaining as much as possible its detection behavior.

A possible formulation of the design problem is to determine a decision region boundary $f(\beta)$ with P_d maximally close to that of $d(\beta)$, while at the same time satisfying the preassigned P_{fa} constraint. We introduce however a more general objective function, in order to take into account also the performance under mismatched conditions, hence in turn to obtain a desired trade-off in this respect. To this end, we select a set of S specifications[1] $\boldsymbol{\rho}_s = [\gamma_s \ \lambda_s \ \psi_s]^{\mathsf{T}}$, $s = 1, \ldots, S$, encoding the desired probabilities of detection ψ_s for each chosen pair of SNR γ_s and mismatch value λ_s and denote by

$$e(f; \boldsymbol{\rho}_s) = \left[P(\tilde{t} > f(\beta) | \gamma = \gamma_s, \cos^2\theta = \lambda_s) - \psi_s\right]^2 \quad (9)$$

[1]We will see later how these specifications can be related to $d(\beta)$.

the squared error between the desired ψ_s and the probability that the detector having decision region boundary $f(\beta)$ will decide for H_1 given γ_s and λ_s. Then, we propose to minimize the weighted least squares cost functional

$$\mathcal{C}_1(f) = \sum_{s=1}^{S} w_s(f; \boldsymbol{\rho}_1, \ldots, \boldsymbol{\rho}_S)\, e(f; \boldsymbol{\rho}_s) \tag{10}$$

with w_s chosen weighting functions. The specifications should be interpreted as "soft desiderata" that will be not necessarily fulfilled in the solution minimizing (10), given their possible conflicting nature.[2] It is worth remarking that $d(\beta)$ is not an unknown but rather an input to the problem, freely chosen by the designer based on the desired behavior. Once chosen, $d(\beta)$ gives the reference to obtain a complete set of performance specifications (as triples of P_d, $\cos^2\theta$, SNR) for both matched and mismatched conditions, to be then fed into $\mathcal{C}_1(f)$. We will discuss in Section IV-C how specification values can be automatically chosen in practice to encode the "desired behavior" given by $d(\beta)$. Moreover, we will specify a weighting strategy in which w_s's depend on both the function $f(\cdot)$ itself and the specifications $\boldsymbol{\rho}_s, s = 1, \ldots, S$.

The infinite-dimensional optimization problem is given by

$$\begin{aligned} &\underset{f \in \mathcal{F}}{\text{minimize}}\ \mathcal{C}_1(f) \\ &\text{s.t. } \mathcal{C}_0(f) = P_{fa} \end{aligned} \tag{11}$$

where $\mathcal{F}$ is a chosen space of functions defined over [0,1], $\mathcal{C}_1(f)$ is given in (10), and

$$\mathcal{C}_0(f) = P(\tilde{t} > f(\beta)|H_0) = 1 - \int_0^1 F_{\tilde{t}|H_0}(f(\beta))p(\beta)\mathrm{d}\beta \tag{12}$$

with $F_{\tilde{t}|H_0}(\cdot)$ denoting the CDF of $\tilde{t}$ under the H_0 hypothesis, and $p(\cdot)$ denoting the pdf of the complex central Beta distribution (better discussed in Section IV-B). The exact solution of such an infinite-dimensional optimization problem would yield the curve that best approximates $d(\beta)$ in the CFAR-FP, i.e., the one minimizing the deviation from the desired behavior expressed through a set of S specification values $\boldsymbol{\rho}_s, s = 1, \ldots, S$. Unfortunately, it involves transcendental functions in both objective function and constraint, making analytical resolution a formidable task.

C. Finite-Dimensional Design Problem

Thus, we focus on a more practical approach which consists in solving a finite-dimensional version of the (intractable) optimization problem (11), where the goal is to approximate the desired decision region boundary $d(\beta)$ through a parametric curve $f(\beta; \boldsymbol{x})$, with $\boldsymbol{x}$ a vector of real parameters. The optimal $\boldsymbol{x}$ that guarantees a preassigned P_{fa} and minimizes the cost function is obtained by solving the optimization problem

$$\begin{aligned} &\underset{\boldsymbol{x}}{\text{minimize}}\ C_1(\boldsymbol{x}) \\ &\text{s.t. } C_0(\boldsymbol{x}) = P_{fa} \end{aligned} \tag{13}$$

where

$$C_1(\boldsymbol{x}) = \sum_{s=1}^{S} w_s(\boldsymbol{x}; \boldsymbol{\rho}_1, \ldots, \boldsymbol{\rho}_S) e(\boldsymbol{x}; \boldsymbol{\rho}_s). \tag{14}$$

Notice that, besides depending on the specifications $\boldsymbol{\rho}_s, s = 1, \ldots, S$, the weights $w_s(\cdot)$ may also depend upon the parametric curve $f(\beta; \boldsymbol{x})$, as in (10), but through the optimization vector $\boldsymbol{x}$. The choice of the quadratic loss

$$e(\boldsymbol{x}; \boldsymbol{\rho}_s) = \left[P(\tilde{t} > f(\beta; \boldsymbol{x})|\gamma = \gamma_s, \cos^2\theta = \lambda_s) - \psi_s\right]^2 \tag{15}$$

is retained and, likewise (12),

$$C_0(\boldsymbol{x}) = P(\tilde{t} > f(\beta; \boldsymbol{x})|H_0) = 1 - \int_0^1 F_{\tilde{t}|H_0}(f(\beta; \boldsymbol{x}))p(\beta)\mathrm{d}\beta. \tag{16}$$

Resolution of the problem above requires to specify the parametric function $f(\beta; \boldsymbol{x})$. In the following, we propose a convenient structure for the latter, which leads to a convenient analytical characterization of the involved statistics. Based on that, a novel reduced-complexity algorithm is devised for designing customized detectors in the CFAR-FP, which is able to find a sub-optimal feasible solution for the optimization problem (13).

Before proceeding, it is worth pointing out that the optimization problem (either in its infinite-dimensional and finite-dimensional version) involved in the design of a customized CFAR detector has an objective function that is specific to a given desired behavior. In fact, the designer's desiderata, expressed in terms of the specifications (P_d, $\cos^2\theta$, SNR) encoding how the desired detector should perform, ultimately determine the actual cost function. As it is not always easy to guess which values of P_d for matched and mismatched levels ($\cos^2\theta$) are feasible and realistically achievable at certain SNRs, a simpler and effective strategy is to assign the desired behavior graphically, leveraging the CFAR-FP properties, and then automatically obtain the specifications from the performance curves of the resulting detector, as illustrated in details in Section IV-C.

IV. Proposed Resolution Approach

A. Choice of Parametric Function $f(\beta; \boldsymbol{x})$

We propose the adoption of a piecewise structure for the parametric function $f(\beta; \boldsymbol{x})$, as follows:

$$f_{\boldsymbol{m}}(\beta; \boldsymbol{\epsilon}) = \sum_{i=1}^{p} f_{m_i}(\beta; \epsilon_i)\, \Pi\left(\frac{\beta - i/p + 1/(2p)}{1/p}\right) \tag{17}$$

with $\boldsymbol{x} = [\boldsymbol{m}^{\mathsf{T}}\ \boldsymbol{\epsilon}^{\mathsf{T}}]^{\mathsf{T}}$, where $\boldsymbol{m} = [m_1\ \cdots\ m_p]^{\mathsf{T}}$ and $\boldsymbol{\epsilon} = [\epsilon_1\ \cdots\ \epsilon_p]^{\mathsf{T}}$. Notice that in general (17) depends on $2p$ parameters to be optimized. For simplicity (and without loss of generality[3]) we have considered a uniform partition of the domain [0,1] in which β takes values and $\{f_{m_i}(\beta; \epsilon_i), i = 1, \ldots, p\}$ is a set of elementary functions to be used in the approximation of $d(\beta)$ according to (13). Among the different

[2]Notice that this way of proceeding is well-founded as it is reminiscent of what happens in other functional approximation problems in signal processing, namely the design of a digital filter or beamformer. In filter design, for instance, the designer first chooses the specific type of function (low-pass, high-pass, with flat top or equi-ripple, etc.) based on the desired behavior, and then addresses the problem of how optimizing its parameters to fulfill the specifications — hence to obtain an approximate solution as close as possible to the desired response but satisfying the constraints.

[3]The proposed approach can be straightforwardly extended to the case of non-uniform partition of the interval [0,1], which could accommodate tighter approximations in certain regions and looser approximations in other ones, according to the $d(\beta)$ at hand.

alternatives, the simplest one is to adopt a piecewise-linear approximation, i.e.,

$$f_{m_i}(\beta;\epsilon_i) = m_i\beta + \epsilon_i. \tag{18}$$

The resolution of the optimization problem (13) will generally lead to a decision region boundary that is discontinuous. If one is interested in having a continuous (piecewise-linear) solution, the optimization problem can be easily extended by adding the following continuity constraint:

$$[\boldsymbol{A}\ \boldsymbol{a}\ \boldsymbol{B}\ \boldsymbol{b}]\begin{bmatrix}\boldsymbol{m}\\ \boldsymbol{\epsilon}\end{bmatrix} = \boldsymbol{0}_{(p-1)\times 1} \tag{19}$$

where $\boldsymbol{A}$ is a $(p-1)$-dimensional bidiagonal matrix with diagonal elements $i/p\,(i=1,\ldots,p-1)$ and upper diagonal elements $-i/p\ (i=1,\ldots,p-2)$, i.e.,

$$\boldsymbol{A} = \begin{bmatrix} \frac{1}{p} & -\frac{1}{p} & 0 & \cdots & 0 \\ 0 & \frac{2}{p} & -\frac{2}{p} & \ddots & \vdots \\ \vdots & 0 & \ddots & \ddots & 0 \\ \vdots & \vdots & \ddots & \ddots & -\frac{p-2}{p} \\ 0 & \cdots & \cdots & 0 & \frac{p-1}{p} \end{bmatrix} \tag{20}$$

and, analogously, $\boldsymbol{B}$ is a $(p-1)$-dimensional bidiagonal matrix with diagonal elements 1 and upper diagonal elements -1, while $\boldsymbol{a}$ and $\boldsymbol{b}$ are $(p-1)$-dimensional vectors with all-zero elements except for the last one, equal to $-\frac{p-1}{p}$ and -1, respectively.

Unfortunately, (13) is highly non-convex and local minima can be abundant, hence the numerical resolution of this problem (with or without continuity constraint) is troublesome. Indeed, as a matter of fact, state-of-the-art global optimization algorithms barely fail in providing even a feasible solution for problem (13). Specifically, different approaches have been tested: an interior-point algorithm initialized with a scatter-search mechanism for generating multiple start points (which is a standard approach to escape local minima [26]), as well as global optimization techniques such as direct methods (e.g., Pattern Search [27], [28]) and genetic algorithms [29], which search over a large portion of the solution space. The results in all our trials, under different conditions and parameter settings, invariably led to unfeasible solutions not satisfying the P_{fa} constraint, and also with very poor performance, far from being an acceptable approximation of the desired $d(\beta)$. To overcome such difficulties, we propose a different optimization strategy that seeks for a feasible solution in a limited, but sufficiently rich subset of the solution space, as detailed below.

For the sake of clarity, it should be noted that the best (and hence desirable) boundary design is in principle the optimal solution to problem (13). Being such a solution not generally available (nor in closed-form, neither using state-of-the-art resolution approaches), in the following we retain the terminology "desired $d(\beta)$" to keep a pointer on an explicit and concrete reference to the desired behavior chosen as input at the initial design stage.

In addition to restricting the set of possible $f(\beta;\boldsymbol{x})$ to piecewise-linear structures of the form in (17), we also reduce the parameter space $\boldsymbol{x}$ from $2p$ to p, by keeping fixed the p parameters in $\boldsymbol{m}$ while optimizing the p parameters in $\boldsymbol{\epsilon}$. This is tantamount to considering a feasible set defined by a piecewise-linear neighborhood of $d(\beta)$ with fixed m_i's. The key aspect of this choice is that on each interval $[(i-1)/p, i/p]$ the approximant function will depend upon a single parameter, i.e., the affine term ϵ_i. In particular, we consider a discontinuous piecewise-linear approximation obtained by juxtaposition of the best linear fitting of $d(\beta)$ in each interval i, as shown in the example reported in Fig. 5, and better discussed later. Following this sub-optimal optimization strategy, we develop a practical algorithm that exploits the piecewise-linear structure of $f_{\boldsymbol{m}}(\beta;\boldsymbol{\epsilon})$ to end up with a low-complexity resolution approach. In doing so, we obtain a feasible solution to the (intractable) original optimization problem, optionally also with continuous boundary.

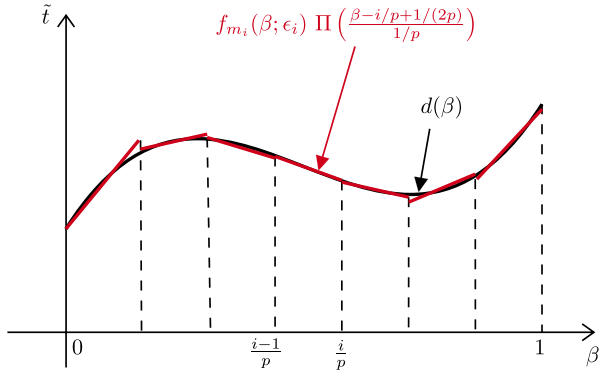

Fig. 5. Example of (17) for $f_{m_i}(\beta;\epsilon_i) = m_i\beta + \epsilon_i$ and $p = 7$.

To start with, (14)–(16) can be made more explicit by exploiting the structure in (17); specifically, for any value of SNR (including $\gamma = 0$, i.e., H_0) and mismatch level (including $\cos^2\theta = 1$, i.e., H_1 under matched conditions), we can write

$$\begin{aligned} P(\tilde{t} > f_{\boldsymbol{m}}(\beta;\boldsymbol{\epsilon})|\gamma,\cos^2\theta) &= 1 - \int_0^1 F_{\tilde{t}|\beta}(f_{\boldsymbol{m}}(\beta;\boldsymbol{\epsilon}))p(\beta)\mathrm{d}\beta \\ &= 1 - \sum_{i=1}^{p} r_i(\epsilon_i,\gamma) \end{aligned} \tag{21}$$

where each term

$$r_i(\epsilon_i,\gamma) = \int_{(i-1)/p}^{i/p} F_{\tilde{t}|\beta}(f_{m_i}(\beta;\epsilon_i))p(\beta)\mathrm{d}\beta \tag{22}$$

is a monotonically increasing one-dimensional function in ϵ_i. Using these new expressions, the optimization problem can be finally recast as

$$\begin{aligned} &\underset{\boldsymbol{\epsilon}}{\text{minimize}}\ C_1(\boldsymbol{\epsilon}) \\ &\text{s.t. } C_0(\boldsymbol{\epsilon}) = P_{fa} \end{aligned} \tag{23}$$

where

$$\begin{aligned} C_1(\boldsymbol{\epsilon}) = &\sum_{h=1}^{S} e(\boldsymbol{\epsilon};\boldsymbol{\rho}_h) \\ &\times \sqrt{\sum\nolimits_{s=1}^{S}\left(e(\boldsymbol{\epsilon};\boldsymbol{\rho}_s) - \frac{1}{S}\sum\nolimits_{j=1}^{S} e(\boldsymbol{\epsilon};\boldsymbol{\rho}_j)\right)^2} \end{aligned} \tag{24}$$

with

$$e(\boldsymbol{\epsilon};\boldsymbol{\rho}_s) = \left[P(\tilde{t} > f_{\boldsymbol{m}}(\beta;\boldsymbol{\epsilon})|\gamma = \gamma_s, \cos^2\theta = \lambda_s) - \psi_s\right]^2$$

and

$$C_0(\boldsymbol{\epsilon}) = P(\tilde{t} > f_{\boldsymbol{m}}(\beta;\boldsymbol{\epsilon})|H_0) = 1 - \sum_{i=1}^{p} r_i(\epsilon_i, 0). \quad (25)$$

The adopted cost function (24) is one among several possible choices, and is aimed at promoting a fairly uniform deviation of the approximated decision region boundary from the desired one, while minimizing the overall approximation error. Details about its derivation and a discussion of alternative choices are reported in Appendix A.

We now provide two key Propositions where the peculiar structure of $f_{\boldsymbol{m}}(\beta;\boldsymbol{\epsilon})$ is exploited together with the statistical characterization of the maximal invariant statistics $(\beta, \tilde{t})$ to derive i) a more compact formula to compute the integral in (22) under the H_1 (matched/mismatched) hypothesis, which will be used to evaluate the cost function in (24); ii) a closed-form solution to the integral appearing in (22) under the H_0 hypothesis, which will be exploited to compute the P_{fa} in (25). Based on such results, we will be able to devise a novel reduced-complexity algorithm for the design of customized detectors according to problem (23). The proposed algorithm will ultimately provide a feasible (though sub-optimal) solution $f_{\boldsymbol{m}}(\beta;\boldsymbol{\epsilon}^*)$ for (23).

B. Analytical Characterization

First recall the general characterization of $(\beta, \tilde{t})$ parameterized in γ and $\cos^2\theta$, which encompasses the one under H_0 (for $\gamma = 0$) and H_1 under matched conditions (for $\cos^2\theta = 1$) [30], see also [2], [6], [22], [31], [32]. The variable $\tilde{t}$ given β is ruled by a complex noncentral $\mathcal{F}$-distribution with 1 and $K - N + 1$ complex degrees of freedom and noncentrality parameter $\gamma\beta\cos^2\theta$, i.e., $\tilde{t} \sim \mathcal{CF}_{1,K-N+1}(\gamma\beta\cos^2\theta)$; β is ruled by a complex noncentral Beta distribution with $K - N + 2$ and $N - 1$ complex degrees of freedom and noncentrality parameter $\gamma(1 - \cos^2\theta)$, i.e., $\beta \sim \mathcal{C}\beta_{K-N+2,N-1}(\gamma(1 - \cos^2\theta))$. We now provide the following results.

Proposition 1: Consider for $f_{\boldsymbol{m}}(\beta;\boldsymbol{\epsilon})$ in (17) the set of affine functions $f_{m_i}(\beta;\epsilon_i) = m_i\beta + \epsilon_i$, $i = 1, \ldots, p$; then, $r_i(\epsilon_i, \gamma)$ in (22) can be more conveniently computed as

$$r_i(\epsilon_i, \gamma) = \int_{(i-1)/p}^{i/p} \Psi(f_{m_i}(\beta;\epsilon_i))\Omega(\beta)\mathrm{d}\beta \quad (26)$$

where

$$\Psi(f_{m_i}(\beta;\epsilon_i)) = (1 + f_{m_i}(\beta;\epsilon_i))^{-(K-N+1)} \times \sum_{\ell=1}^{K-N+1} \binom{K-N+1}{\ell} \frac{f_{m_i}(\beta;\epsilon_i)^\ell}{\Gamma(\ell)} \Gamma\left(\ell, \frac{\delta_F^2}{1 + f_{m_i}(\beta;\epsilon_i)}\right)$$

and

$$\Omega(\beta) = \binom{K}{N-2} \frac{\mathrm{e}^{-\delta_\beta^2}\beta^{K-N+1}}{(1-\beta)^{2-N}} \times {}_1F_1(-K+N-2, N-1, \delta_\beta^2(\beta-1))$$

with $\Gamma(a, b)$ the Euler's upper incomplete Gamma function, ${}_1F_1(a, b; z)$ the Kummer's confluent hypergeometric function, $\delta_F = \gamma\beta\cos^2\theta$ the noncentrality parameter of the F-distribution, and $\delta_\beta = \gamma(1 - \cos^2\theta)$ the noncentrality parameter of the complex Beta distribution.

Proof: See Appendix B, where also the following Corollary is obtained as a by-product. ■

Corollary 1: For negative integer a and positive integer b, ${}_1F_1(a, b; z)$ is a polynomial of degree $-a$ [38, eq. 13.1.3], hence an alternative expression for $\Omega(\beta)$ is

$$\Omega(\beta) = \frac{\mathrm{e}^{-\delta_\beta^2}\beta^{K-N+1}}{(1-\beta)^{2-N}} L_{K-N+2}^{(N-2)}(\delta_\beta^2(\beta-1))$$

where $L_n^{(\alpha)}(x)$ is the generalized Laguerre polynomial of order n and parameter α, here computed in $x = \delta_\beta^2(\beta - 1)$.

Proposition 2: Under the H_0 hypothesis ($\gamma = 0$), the integral appearing in (26) can be solved in closed-form as

$$r_i(\epsilon_i, 0) = F_{\beta|H_0}(i/p) - F_{\beta|H_0}((i-1)/p) - \frac{K!}{(K-N+1)!(N-2)!}\left[g(i/p, \epsilon_i) - g((i-1)/p, \epsilon_i)\right] \quad (27)$$

with $F_{\beta|H_0}(\cdot)$ denoting the CDF of the complex central Beta distribution and

$$g(x, \epsilon_i) = \frac{x}{K-N+2}\left(\frac{x}{1+\epsilon_i}\right)^{K-N+1} \times F_1\left(K-N+2, 2-N, K-N+1, K-N+3; x, \frac{-m_i x}{(1+\epsilon_i)}\right)$$

with $F_1(a, b, c, d; y, z)$ the Appell F_1 function of two variables.

Proof: See Appendix C. ■

C. Low-Complexity Design Procedure

The main challenge with problem (23) is that the joint optimization of the p parameters in $\boldsymbol{\epsilon}$ is still non-trivial as both the cost function and the constraint encode a highly non-linear dependency on the vector $\boldsymbol{\epsilon}$. To circumvent this challenge, we pursue an alternative path that seeks for a feasible solution of (23) by iteratively exploring a range of piecewise-linear approximations of $d(\beta)$. The algorithm takes as inputs the desired decision region boundary $d(\beta)$, the maximum dimension p of the parameter vector $\boldsymbol{\epsilon}$, and the desired P_{fa}, and returns in output the customized piecewise-linear detector $f_{\boldsymbol{m}}(\beta;\boldsymbol{\epsilon}^*)$ working at the preassigned P_{fa}.

The specifications $\boldsymbol{\rho}_s, s = 1, \ldots, S$, have to be chosen in order to correctly encode the desired detection performance under matched and mismatched conditions. To this end, we propose an automatic approach in which the S specifications are directly obtained by sampling the mesa plots of $d(\beta)$, i.e., each $\boldsymbol{\rho}_s$ is set to a point lying on an iso-P_d curve (with level ψ_s) in the SNR-$\cos^2\theta$ plane (with coordinates (γ_s, λ_s)), as shown in Fig. 6. Notice that, since $d(\beta)$ does not generally fulfill the P_{fa} constraint, the specifications obtained by sampling its mesa plots are only indicative of the desired behavior, i.e., they are "soft desiderata" that drive the optimization procedure towards a solution satisfying the P_{fa} constraint while approximating the desired behavior.

The procedure defined above has the advantage of not requiring any ad-hoc setting of the specifications. Moreover, it appears a natural way to make the design requirements in the cost function $C_1(\boldsymbol{\epsilon})$ compatible with the desired $d(\beta)$, facilitating the algorithm in finding a feasible solution $f_{\boldsymbol{m}}(\beta;\boldsymbol{\epsilon})$ that works at the preassigned P_{fa} value. We will refer to such a

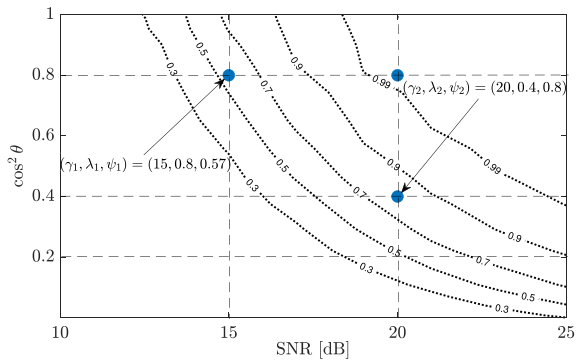

Fig. 6. Proposed strategy for the automatic setting of the S specifications. Mesa plots correspond to $d(\beta)$.

procedure by means of the functional notation $(\boldsymbol{\rho}_1, \ldots, \boldsymbol{\rho}_S) = \text{SampleSpecifications}(d(\beta), S)$.

Once the specifications have been set, the proposed algorithm performs $\sum_{k=2}^{p} k = \frac{p(p+1)}{2} - 1$ iterations in which the function $f_{\boldsymbol{m}}(\beta; \boldsymbol{\epsilon})$ is progressively reparameterized by an increasing number of optimization variables k, ranging from $k = 2$ up to $k = p$. According to the results in Propositions 1 and 2, we consider for $f_{\boldsymbol{m}}(\beta; \boldsymbol{\epsilon})$ the set of affine functions $f_{m_i}(\beta; \epsilon_i) = m_i\beta + \epsilon_i$, $i = 1, \ldots, k$, where the parameters m_i and ϵ_i are initially set equal to the coefficients of the line that approximates (in least squares sense) the desired $d(\beta)$ for $\beta \in [(i-1)/k, i/k]$. In other words, the proposed method explores a range of piecewise-linear approximations of $d(\beta)$ from a coarse ($k = 2$) up to a fine scale ($k = p$).

For each k-dimensional parameterization of $f_{\boldsymbol{m}}(\beta; \boldsymbol{\epsilon})$, our strategy consists in iteratively changing only a single affine parameter ϵ_i at a time, while keeping fixed the remaining $k-1$ elements of the optimization vector $\boldsymbol{\epsilon}$. More specifically, we consider the decomposition of (25) as

$$C_0(\boldsymbol{\epsilon}) = 1 - r_i(\epsilon_i, 0) - \sum_{j=1, j\neq i}^{k} r_j(\epsilon_j, 0).$$

The modified value will then correspond to the root of the equation $C_0(\boldsymbol{\epsilon}) - P_{fa} = 0$ solved with respect to ϵ_i using the result in Proposition 2, that is, the algorithm attempts to modify ϵ_i in order to exactly fulfill the P_{fa} constraint. Among all the configurations of the parametric function $f_{\boldsymbol{m}}(\beta; \boldsymbol{\epsilon})$ satisfying the P_{fa} constraint, we retain as best approximation of $d(\beta)$ the piecewise-linear detector $f_{\boldsymbol{m}}(\beta; \boldsymbol{\epsilon}^*)$ with k^* parameters leading to the minimum value of the cost function $C_1(\boldsymbol{\epsilon})$ in (24), the latter evaluated using the result provided in Proposition 1. Notice that we use the * symbol to remark that the corresponding variables are numerical values resulting from the optimization procedure. The steps of the proposed approach are summarized in Algorithm 1.

Intuitively, the proposed approach consists in deforming only a small portion of the desired decision region boundary $d(\beta)$, but at the same time considering a range of piecewise-linear approximations from coarse to fine scale. This captures the intrinsic trade-off between complexity of the approximate model (in terms of degrees of freedom, while fulfilling exactly P_{fa}) and deviation from the desired performance, the latter expressed through the specifications encoded in the cost function. In doing so, it completely avoids the combinatorial processing intrinsic in the original complex problem at hand. Moreover, the closed-form expressions provided in Propositions 1 and 2 allow the required computation of P_{fa} and P_d to be performed much more quickly as Monte Carlo simulations are avoided.[4]

The proposed algorithm yields, by construction, a (mildly) discontinuous decision region boundary. If one is interested in enforcing an exactly continuous boundary, a further adjustment can be performed, as summarized in Algorithm 2. Each edge of the partition described by the k^* segments returned by Algorithm 1 can be easily made continuous by joining two adjacent

Algorithm 1: Proposed Reduced-complexity Algorithm.

Input: $d(\beta)$, p, P_{fa}
Output: k^*, $f_{\boldsymbol{m}}(\beta; \boldsymbol{\epsilon}^*)$

$(\boldsymbol{\rho}_1, \ldots, \boldsymbol{\rho}_S) = \text{SampleSpecifications}(d(\beta), S)$
for $k = 2$ *to* p **do**
  for $i = 1$ *to* k **do**
    Set $f_{m_i}(\beta; \epsilon_i)$ in eq. (17):

$$f_{m_i}(\beta; \epsilon_i) \leftarrow m_i\beta + \epsilon_i$$

    with m_i, ϵ_i obtained from the linear fitting (regression) of $d(\beta)$ over $\beta \in [(i-1)/k, i/k]$
  end
  for $i = 1$ *to* k **do**
    Compute $\sum_{j=1, j\neq i}^{k} r_j(\epsilon_j, 0)$ using (27)
    Solve $C_0(\boldsymbol{\epsilon}) - P_{fa} = 0$ wrt ϵ_i:

$$\epsilon_i \leftarrow r_i^{-1}\Big(1 - P_{fa} - \sum_{j=1, j\neq i}^{k} r_j(\epsilon_j, 0)\Big)$$

    Evaluate $C_1(\boldsymbol{\epsilon})$ in (24) using (26)
  end
end
Select $[k^*, f_{\boldsymbol{m}}(\beta; \boldsymbol{\epsilon}^*)]$ providing minimum $C_1(\boldsymbol{\epsilon})$

Algorithm 2: Refinement Stage for Obtaining a Continuous Decision Region Boundary.

Input: k^*, $f_{\boldsymbol{m}}(\beta; \boldsymbol{\epsilon}^*)$
Output: Continuous version of $f_{\boldsymbol{m}}(\beta; \boldsymbol{\epsilon}^*)$

Initialize $a_0 \leftarrow \epsilon_1^*$, $a_{k^*} \leftarrow m_{k^*} + \epsilon_{k^*}^*$
for $i = 1$ *to* $k^* - 1$ **do**
  Compute mid-point $a_i \leftarrow (m_i \frac{i}{k^*} + \epsilon_i^* + m_{i+1} \frac{i}{k^*} + \epsilon_{i+1}^*)/2$
  Compute $\delta_i \leftarrow a_i - a_{i-1}$
  Compute $\tilde{m}_i \leftarrow k^*\delta_i$
  Compute $\tilde{\epsilon}_i \leftarrow -i\delta_i + a_i$
end
Update $\tilde{\epsilon}_i \leftarrow \tilde{\epsilon}_i + \epsilon, \forall i$, with $\epsilon \in \mathbb{R}$ such that $C_0(\tilde{\boldsymbol{\epsilon}}) - P_{fa} = 0$ is satisfied

[4]To have an idea, the average time required to find the solution on a standard laptop is about 1.3 seconds for a set of $S = 16$ specifications and for a number of piecewise linear approximations ranging from a coarse ($p = 2$) up to a fine scale ($p = 16$). Such a solution time would be further cut with a low-level implementation, and is thus fully compatible with the operational requirements in case the detectors need to be modified at run-time, e.g., by changing the specifications to include different SNRs and mismatch degrees.

segments in their middle point a_i, given by

$$a_i = \left(m_i \frac{i}{k^*} + \epsilon_i^* + m_{i+1} \frac{i}{k^*} + \epsilon_{i+1}^* \right) /2 \qquad (28)$$

for $i = 1, \ldots, k^* - 1$. The two extreme points corresponding to $\beta = 0$ and $\beta = 1$ are instead kept fixed to their values, that is, $a_0 = \epsilon_1^*$ and $a_{k^*} = m_{k^*} + \epsilon_{k^*}^*$. The resulting continuity-adjusted boundary will have, in each segment, parameters $\tilde{m}_i$ and $\tilde{\epsilon}_i$; they are obtained by modifying the parameters m_i and ϵ_i^* according to the equation of the straight line passing through the points $((i-1)/k^*, a_{i-1})$ and $(i/k^*, a_i)$, i.e.,

$$\tilde{m}_i = \frac{a_i - a_{i-1}}{1/k^*} = k^*(a_i - a_{i-1}) \qquad (29)$$

and

$$\tilde{\epsilon}_i = \frac{i/k^* a_{i-1} - (i-1)/k^* a_i}{1/k^*} = i(a_{i-1} - a_i) + a_i \qquad (30)$$

for $i = 1, \ldots, k^*$, so returning a continuous piecewise-linear version of $f_{\boldsymbol{m}}(\beta; \boldsymbol{\epsilon}^*)$, denoted as $f_{\tilde{\boldsymbol{m}}}(\beta; \tilde{\boldsymbol{\epsilon}})$. Clearly, this refinement stage will (slightly) violate the P_{fa} constraint; however, such a deviation is minor and can be safely recovered by a final vertical shift of the whole curve, until the constraint is exactly satisfied (step 8 in Algorithm 2). Results in the next Section V will show that this procedure, given its minimal impact, does not produce any appreciable performance degradation.

For completeness, we explicitly report the decision test of a generic customized detector $f_{\boldsymbol{m}}(\beta; \boldsymbol{\epsilon}^*)$ designed by means of the procedure discussed above (the same applies to the continuous version $f_{\tilde{\boldsymbol{m}}}(\beta; \tilde{\boldsymbol{\epsilon}})$):

$$\begin{matrix} H_1 \\ \tilde{t} \gtrless \\ H_0 \end{matrix} f_{\boldsymbol{m}}(\beta; \boldsymbol{\epsilon}^*) = \begin{cases} m_1\beta + \epsilon_1^* & 0 \le \beta < \frac{1}{k^*} \\ \vdots & \vdots \\ m_{k^*}\beta + \epsilon_{k^*}^* & \frac{k^*-1}{k^*} < \beta \le 1 \end{cases} . \qquad (31)$$

Moreover, in Algorithm 3 we report the corresponding detection rule for a given realization of the maximal invariant statistics $(\beta, \tilde{t})$, computed from the observed data $\boldsymbol{z}, \boldsymbol{z}_1, \ldots, \boldsymbol{z}_K$. As for the parameters $(m_\ell, \epsilon_\ell^*)$, they correspond to a specific pair selected among the k^* pairs (m_i, ϵ_i^*), $i = 1, \ldots, k^*$, that constitute $f_{\boldsymbol{m}}(\beta; \boldsymbol{\epsilon}^*)$. The detector simply finds the specific interval $[(\ell-1)/k^*, \ell/k^*]$ in which the β statistic falls among the k^* cases in (31), and then uses the corresponding parameters $(m_\ell, \epsilon_\ell^*)$ to test whether the $\tilde{t}$ statistic exceeds the corresponding threshold $\eta_\ell = m_\ell \beta + \epsilon_\ell^*$ (decide for H_1) or not (decide for H_0). A convenient interpretation of the detection rule can be visualized in the CFAR-FP as testing whether the $\tilde{t}$ statistic falls above or below the line with parameters $(m_\ell, \epsilon_\ell^*)$, which represents the portion of the decision region boundary to be considered for that specific realization of β.

V. Performance Assessment

In this section, we assess the performance of the two examples of radar detectors discussed in Section III, whose design is obtained through the methodology proposed in Section IV. The analysis is performed on both simulated and real-world radar data. The design is conducted assuming a maximum number of segments for partitioning the domain $\beta \in [0, 1]$ set to $p = 16$.

Thresholds are set by Monte Carlo simulation with $100/P_{fa}$ independent trials. For target simulation, we assume $\boldsymbol{v} = [1 \ e^{j2\pi f_d} \ \ldots \ e^{j2\pi(N-1)f_d}]^\mathsf{T}$ with a normalized Doppler frequency $f_d = 0.08$ (a small value such that the target competes with low pass clutter). To model a mismatched target, we define the actual steering vector $\boldsymbol{p}$ as $\boldsymbol{v}$ but with $f_d + \delta_f$ and δ_f varying in order to obtain different levels of mismatches.

Algorithm 3: Detection Rule of the Customized Detector.

Input: $\tilde{t}$, β, k^*, $f_{\boldsymbol{m}}(\beta; \boldsymbol{\epsilon}^*)$
Output: Decision for H_0 or H_1

1: Find index ℓ such that $\beta \in [(\ell-1)/k^*, \ell/k^*]$;
2: Detection rule:

$$\begin{matrix} H_1 \\ \tilde{t} \gtrless \\ H_0 \end{matrix} m_\ell \beta + \epsilon_\ell^*$$

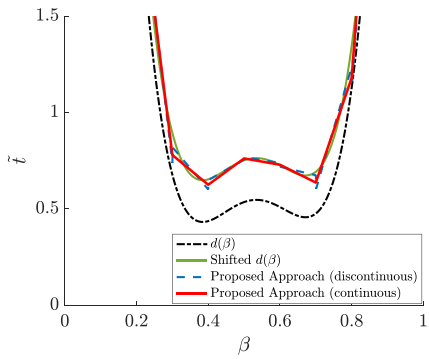

Fig. 7. CFAR-FP for the case of the double-well detector.

A. Performance of the Double-Well Detector

We start by analyzing the first example of detector design presented in Section III, labeled "double-well". We consider $N = 16$, $K = 32$, and a desired $P_{fa} = 10^{-4}$. As to $\boldsymbol{C}$, we consider the sum of a Gaussian-shaped clutter and white (thermal) noise 10 dB weaker, i.e., $\boldsymbol{C} = \boldsymbol{R}_c + \sigma_n^2 \boldsymbol{I}_N$ with the (m_1, m_2)th element of the matrix $\boldsymbol{R}_c$ given by $[\boldsymbol{R}_c]_{m_1,m_2} = \exp\{-2\pi^2\sigma_f^2(m_1 - m_2)^2\}$ and $\sigma_f \approx 0.051$ (corresponding to a one-lag correlation coefficient of the clutter component equal to 0.95). Finally, we consider 10^3 independent trials to compute the P_d.

The $d(\beta)$ of Section III has a $P_{fa} \approx 10^{-3}$, which is about an order of magnitude greater than the desired P_{fa}. The automatic settings of the specifications is carried out by sampling the SNR-$\cos^2\theta$ plane of the $d(\beta)$ mesa plots over four uniformly spaced values of the mismatch, namely $\lambda_s \in \{1, 0.75, 0.5, 0.25\}$, and over four different values of SNR $\gamma_s \in \{8, 10, 15, 20\}$, for a total of $S = 16$ specifications.

1) Analysis of the Decision Region Boundary Approximation: In Fig. 7, we depict the decision region boundary $f_{\boldsymbol{m}}(\beta; \boldsymbol{\epsilon}^*)$ of the double-well detector obtained through the proposed approach, which for this case returned a $f_{\boldsymbol{m}}(\beta; \boldsymbol{\epsilon}^*)$ with $k^* = 10$ segments. For comparison, the decision region boundary of the detector obtained by simply shifting $d(\beta)$ to match the preassigned P_{fa} is reported, labeled as "Shifted $d(\beta)$" for brevity. As it can be noticed, the proposed approach provides a decision region boundary which is close to that of the shifted $d(\beta)$, for both the discontinuous and continuous versions. Indeed, the discontinuity gaps at the junctions of the different segments are very limited, so if one is interested in having a continuous

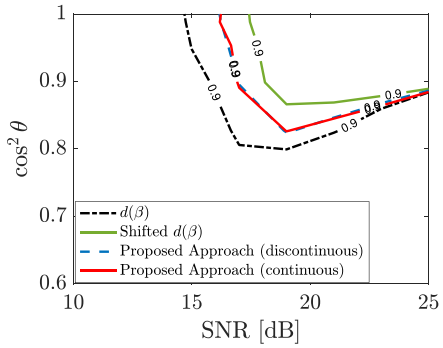

Fig. 8. Detection performance of the desired $d(\beta)$ in comparison to the shifted $d(\beta)$ and to the proposed approach (with either continuous or discontinuous decision region boundary) at $P_d = 0.9$.

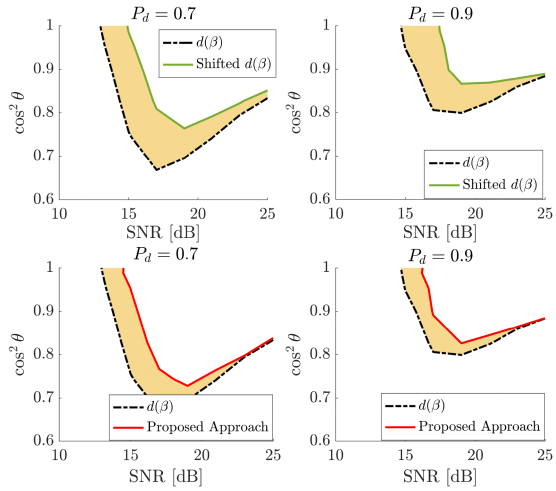

Fig. 9. Areas between iso-P_d curves (AbI) for the proposed approach, in comparison with the shifted $d(\beta)$ detector.

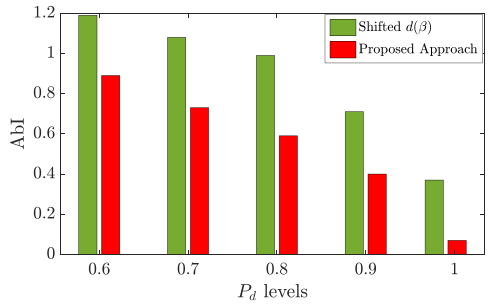

Fig. 10. Areas between iso-P_d curves (AbI) of the double-well detectors as a function of the P_d levels.

boundary the solution $f_{\boldsymbol{m}}(\beta;\boldsymbol{\epsilon}^*)$ provided by Algorithm 1 can be safely made continuous through the refinement stage described in Algorithm 2, without compromising the performance of the design. The latter remarkable fact is not apparent from Fig. 7 but can be appreciated by looking at the mesa plots of the different detectors, as discussed below.

2) Comparison Between Continuous and Discontinuous Solutions: In Fig. 8, we report the detection performance of the proposed double-well detector in the SNR-$\cos^2\theta$ plane for a single level of $P_d = 0.9$, also in comparison with the desired $d(\beta)$ and with the shifted $d(\beta)$. It can be seen that the proposed double-well detector follows more closely the behavior of the desired $d(\beta)$, with an evident gap compared to the performance of the shifted $d(\beta)$. This confirms the validity of the proposed algorithm: by exploring a range of k-segment piecewise-linear approximations of the desired $d(\beta)$ from a coarse ($k = 2$) up to a fine scale ($k = p = 16$), our design approach is able to provide a satisfactory trade-off between satisfaction of the P_{fa} constraint and deviation from the desired performance in terms of P_d under matched and mismatched conditions. From Fig. 8 it also emerges that the minimal changes required to make the decision region boundary $f_{\boldsymbol{m}}(\beta;\boldsymbol{\epsilon}^*)$ continuous practically lead to zero deviations from the detection performance of the discontinuous case; therefore, in the following we will no longer consider such a distinction. The competitor "shifted $d(\beta)$" provides instead a much worse approximation of the desired $d(\beta)$; this may appear counterintuitive, since in Fig. 7 the decision region boundaries of the three detectors look quite close to each other. But this is exactly the motivation of this work, as discussed in Section II: given the highly-nonlinear mapping between the maximal invariant statistics (CFAR-FP) and the corresponding detection performance under matched and mismatched conditions (mesa plots), it is challenging to adjust the desired $d(\beta)$ so that the P_{fa} constraint can be fulfilled without jeopardizing the design, as far as possible.

3) Analysis of the Deviation From the Desired Behavior: It is worth remarking that the desired $d(\beta)$ does not share the same P_{fa} of the other detectors ($d(\beta)$ is working at a P_{fa} which is about an order of magnitude greater), hence it cannot be strictly considered as a benchmark for the desired P_d, but only for its behavior, which should be approximated as closely as possible. For a better assessment, we consider as metric the area of the planar region delimited by the iso-P_d curves of a given detector and that of the $d(\beta)$ in the SNR-$\cos^2\theta$ plane, which measures the level of closeness between such curves. In fact, the smaller the gap from the iso-P_d curves of $d(\beta)$, the better the approximation of the desired behavior under both matched and mismatched conditions. We will refer to such a metric as "area between iso-P_d curves" (AbI).

In Fig. 9 we highlight the AbI of the proposed detector in comparison with the AbI of the shifted $d(\beta)$, for two different levels of $P_d = \{0.7, 0.9\}$. Results demonstrate that the double-well detector provides a better approximation of the desired $d(\beta)$, being its corresponding areas visibly smaller than those of the shifted $d(\beta)$ detector. More precisely, Fig. 10 shows the exact values of the AbI as a function of the P_d levels. Remarkably, the proposed double-well detector satisfactorily follows the detection performance of the desired $d(\beta)$ for all the considered P_d levels, with an approximation error that tends to decrease for higher values of the P_d.

4) Analysis of the Detection Performance: In Fig. 11, we compare the double-well detector against state-of-the-art detectors. Since the former customized detector aims at rejecting mismatched signals while preserving high detection power under matched conditions, we have included as relevant competitors the well-known Kelly's detector, which is taken as a reference for the performance under matched conditions, as well as the ACE, WABORT and RAO detectors, which are instead taken as benchmarks for the performance under mismatched conditions. It is interesting to observe that the double-well detector guarantees almost the same P_d of Kelly's detector under matched conditions, while providing much higher levels of selectivity. Furthermore, it is much more powerful than ACE and exhibits higher rejection capabilities for large SNR values. It is also remarkable

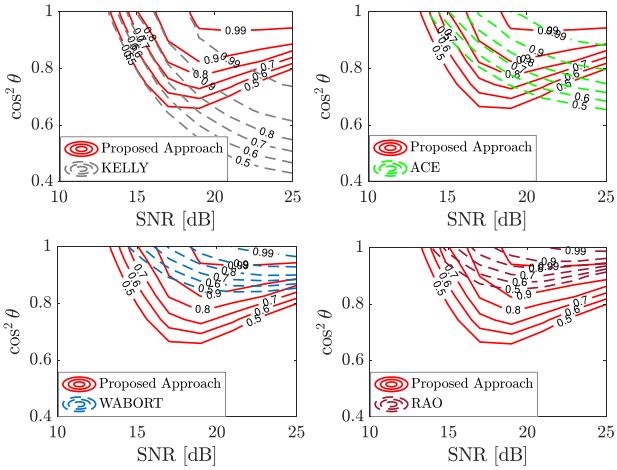

Fig. 11. Mesa plots of the double-well detector compared to Kelly, ACE, WABORT and RAO detectors.

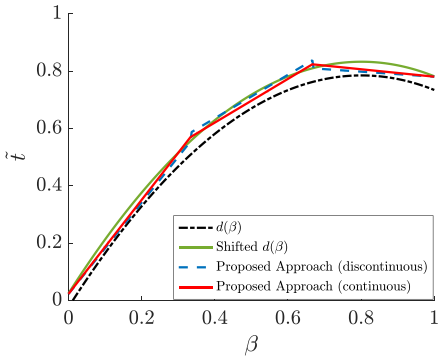

Fig. 12. CFAR-FP for the case of the combined AMF-ROB detector.

to notice that, compared to the very selective WABORT and RAO detectors, the double-well detector does not experience any significant P_d loss under matched conditions, while still preserving satisfactory rejection capabilities. In summary, the detector designed by the proposed methodology achieves a P_d similar to Kelly's detector but it is much more selective, which is a major achievement since state-of-the-art selective detectors typically experience a P_d loss compared to Kelly's detector.

B. Performance of the Combined AMF-ROB Detector

For further illustration, we analyze also the second example of detector design presented in Section III, namely the case in which the desired $d(\beta)$ is obtained by combining the decision region boundaries of the two well-known detectors AMF and ROB. For the analysis, we consider the same parameters as in Section V-A. Intuitively, this scenario appears to be more favorable since the desired $d(\beta)$ exhibits a $P_{fa} = 2.6 \cdot 10^{-4}$, which is already quite close to the final desired P_{fa}. The specifications $\boldsymbol{\rho}_s$ are automatically set by sampling the SNR-$\cos^2\theta$ plane of the desired $d(\beta)$ mesa plots at the same coordinates of the previous example in Section V-A.

1) Analysis of the Decision Region Boundary Approximation: Fig. 12 depicts the decision region boundary of the combined detector obtained through the proposed reduced-complexity algorithm, in comparison with the desired $d(\beta)$ and with the decision region boundary of the shifted $d(\beta)$. Among the explored configurations of $k \in [2, 16]$, the best value of the objective function

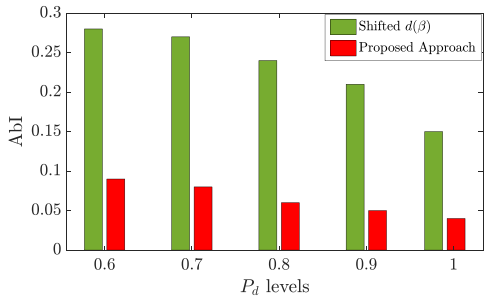

Fig. 13. Areas between iso-P_d curves (AbI) of the combined AMF-ROB detectors as a function of the P_d levels.

is achieved for $k^* = 3$, namely the configuration in which the decision region boundary $f_{\boldsymbol{m}}(\beta; \boldsymbol{\epsilon}^*)$ consists of a juxtaposition of three linear segments approximating the positive-slope line of AMF for the lower range of β and attaining ROB's behavior in the upper range.

2) Comparison Between Continuous and Discontinuous Solutions: Also in this case, the discontinuities in $f_{\boldsymbol{m}}(\beta; \boldsymbol{\epsilon}^*)$ are very limited, as confirmed by the continuous version of the decision region boundary, which practically coincides with its discontinuous version. As for the previous case (double-well detector), the decision region boundaries of the detectors are close to each other, and in this case also closer to the desired $d(\beta)$ since the P_{fa} of the latter is already near the design value. However, again, a small difference in the boundary can produce a non-negligible impact on the performance.

3) Analysis of the Deviation From the Desired Behavior: Specifically, to assess the adherence of the combined detector to the behavior of the desired $d(\beta)$, in Fig. 13 we report the AbI values as a function of the P_d levels. Results demonstrate that the proposed approach is able to provide a more accurate approximation of the desired $d(\beta)$ compared to the shifted $d(\beta)$, even in this more favorable scenario in which the P_{fa} of the desired $d(\beta)$ is very close to the preassigned one. As a whole, the use of the proposed methodology can yield closer approximations of a desired detector $d(\beta)$ for a prefixed P_{fa} compared to the mere shift of $d(\beta)$ itself, regardless of the extent of the gap between initial and desired P_{fa} values.

4) Analysis of the Detection Performance: For completeness, we finally report in Fig. 14 the performance of the proposed combined detector, in comparison to the performance of the AMF, ROB, and Kalson detectors. It is worth noting that the proposed detector is able to combine the satisfactory robustness of the AMF with the high detection power of the ROB under matched conditions (which is practically the same as Kelly's detector). Specifically, it is as powerful as both ROB and Kalson under matched conditions, while guaranteeing at the same time the level of robustness of AMF under mismatched conditions, which is in between ROB and Kalson.

C. Evaluation on Real Radar Data

To corroborate the above results, we have carried out a performance evaluation on real radar measurements by considering the L-band land clutter data collected by the Phase One radar at the Katahdin Hill site, MIT Lincoln Laboratory. We used the dataset contained in the *"H067038.3"* file, which is composed of 30720 temporal returns from 76 range cells with HH polarization [33], [34]. Given that the total number of real clutter measurements

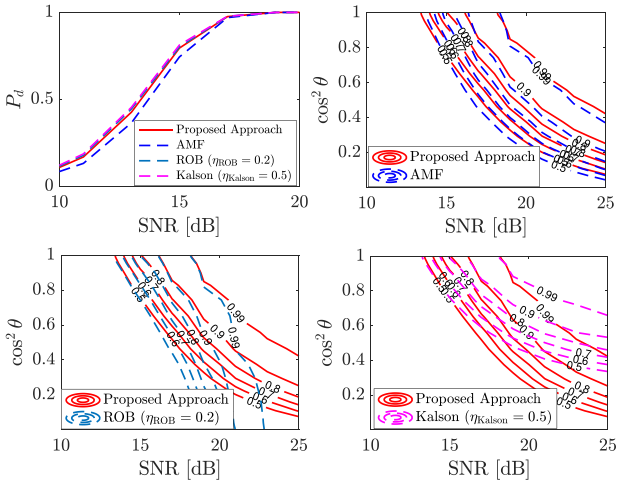

Fig. 14. Mesa plots of the combined AMF-ROB detector compared to the AMF, ROB, and Kalson detectors.

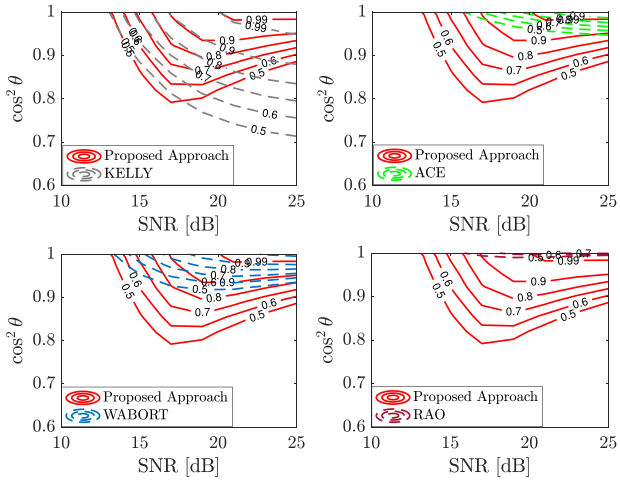

Fig. 15. Mesa plots of the double-well detector compared to Kelly, ACE, WABORT and RAO detectors for $N = 4$, $K = 8$, evaluated on the Phase One dataset.

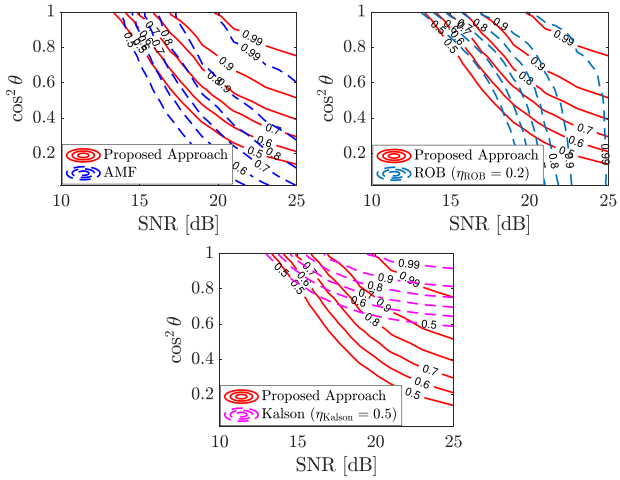

Fig. 16. Mesa plots of the combined AMF-ROB detector compared to the AMF, ROB, and Kalson detectors for $N = 4$, $K = 8$, evaluated on the Phase One dataset.

is not sufficient to guarantee a number of snapshots matching the $100/P_{fa}$ rule for the value of $P_{fa} = 10^{-4}$ assumed in the simulation analyses, we readjusted the design of the two proposed detectors by downscaling it to $N = 4$, $K = 8$, and a desired $P_{fa} = 10^{-3}$. All the remaining parameters are instead kept the same.

For both the double-well and combined AMF-ROB CFAR detectors, the decision region boundaries obtained through the proposed low-complexity design procedure show a very good match with the desired ones (figures omitted for conciseness), confirming the general validity of our approach, which can flexibly adapt to a new set of parameters. In the following we report the analysis of the corresponding performance.

We start the evaluation by estimating the actual P_{fa} of the detectors when operating on the Phase One dataset. All the detectors thresholds are set to guarantee the desired $P_{fa} = 10^{-3}$ on simulated data. For the analysis, we select the 30-th range cell as the CUT and $K/2$ adjacent range cells on each side of the CUT as secondary data. We construct the data vectors by selecting N consecutive pulses from each range cell, with 1 pulse of overlap in order to obtain 10^4 different snapshots. The proposed double-well detector exhibits a $P_{fa} = 5 \cdot 10^{-4}$, a value that does not deviate too much from the nominal one and, remarkably, is even lower. Kelly and ACE detectors share the same value of $P_{fa} = 5 \cdot 10^{-4}$, while WABORT and RAO exhibit a $P_{fa} = 9 \cdot 10^{-4}$. Interestingly, all the selective detectors share very similar values of P_{fa}, which well approximate the nominal one. Analogous results have been obtained for the case of robust detectors: specifically, the combined AMF-ROB, AMF, and ROB detectors also exhibit a $P_{fa} = 5 \cdot 10^{-4}$, while Kalson has a $P_{fa} = 4 \cdot 10^{-4}$.

The performances in terms of P_d are then evaluated by adding to the CUT a synthetic target $\alpha \boldsymbol{v}$, as done for the simulated data. To make the comparison precisely fair, we adjusted the thresholds of the WABORT, RAO, and Kalson so as to match the same $P_{fa} = 5 \cdot 10^{-4}$ of the other detectors. In Fig. 15 and Fig. 16, we compare the performance of the proposed double-well and combined AMF-ROB detectors against the same state-of-the-art competitors considered in Section V-A and Section V-B. As it can be noticed, the proposed design procedure confirms its effectiveness in correctly approximating the desired CFAR behaviors, with the proposed double-well detector that preserves the high P_d of the Kelly's detector under matched conditions, while striking a more evident selectivity under mismatched conditions. Remarkably, the gain in terms of P_d under matched conditions becomes much more pronounced compared to the ACE and RAO detectors, which turn out to be very selective. Similarly, the proposed combined AMF-ROB detector practically keeps the satisfactory robustness of the AMF detector, while guaranteeing the high detection power of the ROB under matched conditions. Its robust behavior still lies between ROB and Kalson, confirming the same findings on simulated data.

VI. Conclusion

The paper proposed a methodology for the design of customized CFAR detectors in Gaussian disturbance, with desired behavior in terms of robustness or selectivity, and working at a preassigned P_{fa} value. By exploiting a reinterpretation of CFAR detection in a suitable feature plane based on maximal invariant statistics (CFAR-FP), the optimal approximation problem has

been formulated and analyzed. To overcome its analytical and numerical intractability, a general reduced-complexity approach has been developed, which seeks for a sub-optimal solution in a restricted, but sufficiently rich feasible set. The proposed algorithm is very efficient in finding a detector satisfying the requirements and provides satisfactory performance.

Under this framework, two novel customized detectors have also been designed and analyzed, for illustration purposes. The first one starts from a desired curve directly drawn in the CFAR-FP, whose shape allows for rejection of mismatched signals, but at the same time leads to high detection power under matched conditions. The second design example follows instead a strategy that combines two existing detectors, with the aim of taking the best from both. Specifically, being the ROB detector practically as powerful as Kelly's detector but very robust, we used a combination of AMF (which has a lower robustness) and ROB to find a good balance. The same approach can work for the selective case, by appropriate choice of the detectors to combine.

Future work includes the investigation of alternative resolution approaches for problem (11) that can consider additional feasible solutions. Another interesting possibility is to extend the proposed framework to environments different from the homogeneous Gaussian one, using a different set of proper maximal invariant statistics [35], [36], [37].

Appendix A
Weighting Strategies

As to the weights $w_s \in [0,1]$, different strategies can be identified to end up with an objective function able to encode the different design requirements (and their relative priority) in the proper way, summarized as follows:

- $w_s = 1, \forall s$
- $w_s = w(\gamma_s, \lambda_s)$
- $w_s = w(\boldsymbol{\epsilon}; \boldsymbol{\rho}_1, \ldots, \boldsymbol{\rho}_S), \forall s$.

The first option considers constant weights, hence is tantamount to having an (unweighted) least squares functional, which will treat all the S specifications $\boldsymbol{\rho}_s$ equally. As a consequence, errors on higher probabilities of detection will have a dominant effect, being their impact on the objective function greater in magnitude.

The second option considers diversified weights given by a weighting function $w(\cdot)$ depending only on SNR and match/mismatch level specifications; its definition impacts on the relative priority given to the different specifications. The choice $w_s = 1/\psi_s^2$ has the special meaning of a relative error, thus would overcome the limitation of the first option ($w_s = 1\,\forall s$). However, it would produce the opposite effect of giving too much weight to errors on low values of the probability of detection (under matched or mismatched conditions), which may be detrimental to the detection power for higher SNRs (an unacceptable behavior for a radar detector). So, other choices should be identified, e.g. an increasing function of λ_s, possibly constant in (a certain range of) γ_s. In fact, $w_s = \lambda_s$ (or λ_s^α, $\alpha > 0$, to also adjust the decay rate) would promote more priority to maximizing P_d for any value of SNR, but at the same time would take into account the desired probability of deciding for H_1 under various level of mismatches. For $S = 1$ with $\lambda_1 = 1$, $\psi_1 = 1$, and a chosen SNR γ_1, the minimization of $\mathcal{C}_1(\boldsymbol{\epsilon})$ would be equivalent to the maximization of

$$P_d = P\left(\tilde{t} > f_{\boldsymbol{m}}(\beta;\boldsymbol{\epsilon})|\gamma_1, 1\right) = 1 - \int_0^1 F_{\tilde{t}|\beta,H_1}\left(f_{\boldsymbol{m}}(\beta;\boldsymbol{\epsilon})|\gamma_1\right) p(\beta)\mathrm{d}\beta$$

where $F_{\tilde{t}|\beta,H_1}(\cdot)$ is the CDF of $\tilde{t}$ given β under the H_1 hypothesis, hence the Neyman-Pearson inspired rationale is retrieved. A slight generalization of this formulation is the maximization of P_d in a span of SNRs, with weights all equal or increasing/decreasing according to the given priority to the high/low SNR regime.

In general, the main drawback of the second weighting strategy ($w_s = w(\gamma_s, \lambda_s)$) is that a fine-tuning of the weights is necessary, whose impact may be not completely predictable, thus resulting in a trial-and-error effort. For this reason, we adopt the third strategy, in which weights are all equals but set to a certain function $w(\boldsymbol{\epsilon}; \boldsymbol{\rho}_1, \ldots, \boldsymbol{\rho}_S)$ that depends on all specifications as well as on the optimization parameters $\boldsymbol{\epsilon}$. A simplifying yet reasonable choice is to map such dependencies into the error function $e(\cdot)$ as

$$w = \frac{1}{S}\underbrace{\sqrt{\frac{1}{S-1}\sum\nolimits_{s=1}^{S}\left(e(\boldsymbol{\epsilon};\boldsymbol{\rho}_s) - \bar{e}(\boldsymbol{\epsilon};\boldsymbol{\rho}_1,\ldots,\boldsymbol{\rho}_S)\right)^2}}_{\sigma_e} \quad (32)$$

where $\bar{e}(\boldsymbol{\epsilon};\boldsymbol{\rho}_1,\ldots,\boldsymbol{\rho}_S) = 1/S\sum_{j=1}^{S} e(\boldsymbol{\epsilon};\boldsymbol{\rho}_j)$ and σ_e denotes the empirical standard deviation of the squared error. By substituting this expression into (14), we finally obtain (24).

Appendix B
Proof of Proposition 1

We start from $\Psi(f_{m_i}(\beta;\epsilon_i))$, which can be obtained as a more convenient rewriting of $F_{\tilde{t}|\beta}(f_{m_i}(\beta;\epsilon_i))$. More precisely, we recall that in the general case [22]

$$F_{\tilde{t}|\beta}(f_{m_i}(\beta;\epsilon_i)) = \frac{f_{m_i}(\beta;\epsilon_i)}{(1+f_{m_i}(\beta;\epsilon_i))^{K-N+1}}\sum_{k=0}^{K-N}\binom{K-N+1}{1+k} \times (f_{m_i}(\beta;\epsilon_i))^k \mathrm{e}^{-\frac{\delta_F^2}{1+f_{m_i}(\beta;\epsilon_i)}}\sum_{i=0}^{k}\left(\frac{\delta_F^2}{1+f_{m_i}(\beta;\epsilon_i)}\right)^i\frac{1}{i!}.$$

We then notice that, by manipulating from [38, eq. 6.5.13] the innermost summation can be expressed in terms of Eulerian complete and upper incomplete gamma functions as

$$\sum_{i=0}^{k}\left(\frac{\delta_F^2}{1+f_{m_i}(\beta;\epsilon_i)}\right)^i\frac{1}{i!} = \mathrm{e}^{\frac{\delta_F^2}{1+f_{m_i}(\beta;\epsilon_i)}}\frac{\Gamma\left(1+k,\frac{\delta_F^2}{1+f_{m_i}(\beta;\epsilon_i)}\right)}{\Gamma(1+k)}.$$

The ultimate $\Psi(f_{m_i}(\beta;\epsilon_i))$ follows by plugging back the above expression in $F_{\tilde{t}|\beta}(f_{m_i}(\beta;\epsilon_i))$ and by performing a change of variable $1+k=\ell$.

Similarly, $\Omega(\beta)$ can be obtained by a proper rewriting of $p(\beta)$. Specifically, we recall that

$$p(\beta) = \frac{\mathrm{e}^{-\delta_\beta^2\beta}\beta^{K-N+1}}{(1-\beta)^{2-N}}\frac{\Gamma(K+1)}{\Gamma(K-N+2)}\sum_{j=0}^{K-N+2}\binom{K-N+2}{j}$$

$$\times \frac{1}{(N+j-2)!}\delta_\beta^{2j}(1-\beta)^j.$$

The expression of $\Omega(\beta)$ can be derived by exploiting the similarity between the above summation and the generalized Laguerre polynomials $L_n^{(\alpha)}(x)$ of order $n = K-N+2$ for $\alpha = N-2$; in particular, by using [38, eq. 13.6.9] together with [38, eq. 22.3.9] it is possible to write the following identity:

$$\sum_{j=0}^{K-N+2}(-1)^j\binom{K}{K-N+2-j}\frac{x^j}{j!} = \binom{K}{N-2}{}_1F_1(-K+N-2, N-1; x).$$

Then, noticing that binomial/factorial terms in the two expressions can be related as

$$\frac{\binom{K-N+2}{j}}{(N+j-2)!} = \binom{K}{K-N+2-j}\frac{(K-N+2)!}{K!j!}$$

and that $(1-\beta)^j = (-1)^j(\beta-1)^j$, we obtain for $x = \delta_\beta^2(\beta-1)$

$$\sum_{j=0}^{K-N+2}\frac{\binom{K-N+2}{j}}{(N+j-2)!}\delta_\beta^{2j}(1-\beta)^j = \frac{1}{\Gamma(N-1)}{}_1F_1(-K+N-2, N-1; \delta_\beta^2(\beta-1))$$

since $\frac{(K-N+2)!}{K!}\binom{K}{N-2} = \frac{1}{(N-2)!} = \frac{1}{\Gamma(N-1)}$. The thesis follows by substituting back into $p(\beta)$ and recognizing that $\frac{\Gamma(K+1)}{\Gamma(K-N+2)\Gamma(N-1)} = \binom{K}{N-2}$.

Appendix C
Proof of Proposition 2

Under the H_0 hypothesis, we have that

$$r_i(\epsilon_i) = \int_{(i-1)/p}^{i/p}\frac{f_{m_i}(\beta;\epsilon_i)}{(1+f_{m_i}(\beta;\epsilon_i))^{K-N+1}}\sum_{j=0}^{K-N}\binom{K-N+1}{1+j} \times (f_{m_i}(\beta;\epsilon_i))^j p(\beta)\mathrm{d}\beta.$$

By using a change of variable $1+j = z$ and noting that by the algebraic binomial formula $\sum_{z=0}^{K-N+1}\binom{K-N+1}{z}(f_{m_i}(\beta;\epsilon_i))^z = (1+f_{m_i}(\beta;\epsilon_i))^{K-N+1}$, $r_i(\epsilon_i)$ can be recast as

$$r_i(\epsilon_i) = \int_{(i-1)/p}^{i/p}p(\beta)\mathrm{d}\beta - \left(\int_0^{i/p}(1+f_{m_i}(\beta;\epsilon_i))^{-(K-N+1)}p(\beta)\mathrm{d}\beta - \int_0^{(i-1)/p}(1+f_{m_i}(\beta;\epsilon_i))^{-(K-N+1)}p(\beta)\mathrm{d}\beta\right).$$

Considering the integrals between braces, for $u = i/p$ or $u = (i-1)/p$ we have

$$\int_0^u(1+f_{m_i}(\beta;\epsilon_i))^{-(K-N+1)}p(\beta)\mathrm{d}\beta = \frac{K!}{(N-2)!(K-N+1)!} \times \int_0^u(1+\epsilon_i+m_i\beta)^{-(K-N+1)}\beta^{K-N+1}(1-\beta)^{N-2}\mathrm{d}\beta$$

which is a generalization of the integral definition of the Euler's Beta function; in particular, it can be computed by exploiting the following identity

$$\int_0^u\frac{x^n(1-x)^m}{(1+ax)^n}\mathrm{d}x = \frac{x^{n+1}}{n+1}F_1(n+1, -m, n, n+2; u, -au)$$

which is valid for $a > 0$ (for $a = 0$ returns the Beta function) and $0 \le u \le 1$, m and n positive integers, where $F_1(a,b,c,d;y,z)$ is the Appell F_1 (hypergeometric) function of two variables [39, sec. 9.18].

The result of Proposition 2 follows by noting that $\int_{(i-1)/p}^{i/p}p(\beta)\mathrm{d}\beta = F_{\beta|H_0}(i/p) - F_{\beta|H_0}((i-1)/p)$ and exploiting the identity above for $a = m_i/(1+\epsilon_i)$, $m = N-2$, and $n = K-N+1$, i.e.,

$$\int_0^u(1+f_{m_i}(\beta;\epsilon_i))^{-(K-N+1)}p(\beta)\mathrm{d}\beta = \frac{u}{K-N+2}\left(\frac{u}{1+\epsilon_i}\right)^{K-N+1} \times F_1\left(K-N+2, 2-N, K-N+1, K-N+3; u, \frac{m_i u}{1+\epsilon_i}\right)$$

hence the thesis follows straight.

Acknowledgment

The authors would to thank Prof. J. B. Billingsley, MIT Lincoln Lab, for the Phase One L-band clutter data.

References

[1] L. E. Brennan and L. S. Reed, "Theory of adaptive radar," *IEEE Trans. Aerosp. Electron. Syst.*, vol. AES-9, no. 2, pp. 237–252, Mar. 1973.
[2] E. J. Kelly, "An adaptive detection algorithm," *IEEE Trans. Aerosp. Electron. Syst.*, vol. AES-22, no. 2, pp. 115–127, Mar. 1986.
[3] W. Liu, J. Liu, C. Hao, Y. Gao, and Y. L. Wang, "Multichannel adaptive signal detection: Basic theory and literature review," *Sci. China Inf. Sci.*, vol. 65, no. 2, pp. 1–40, Jan. 2022.
[4] C. Hao, D. Orlando, J. Liu, and C. Yin, *Advances in Adaptive Radar Detection and Range Estimation*, Singapore: Springer, 2022.
[5] A. Coluccia, G. Ricci, and C. D. Richmond, "Adaptive radar detection without secondary data for uncooperative spectrum sharing scenarios," *IEEE Trans. Signal Process.*, vol. 69, pp. 3206–3219, 2021.
[6] E. J. Kelly, "Performance of an adaptive detection algorithm; rejection of unwanted signals," *IEEE Trans. Aerosp. Electron. Syst.*, vol. 25, no. 2, pp. 122–133, Mar. 1989.
[7] F. C. Robey, D. L. Fuhrman, E. J. Kelly, and R. Nitzberg, "A CFAR adaptive matched filter detector," *IEEE Trans. Aerosp. Electron. Syst.*, vol. 29, no. 1, pp. 208–216, Jan. 1992.
[8] S. Kraut and L. L. Scharf, "The CFAR adaptive subspace detector is a scale-invariant GLRT," *IEEE Trans. Signal Process.*, vol. 47, no. 9, pp. 2538–2541, Sep. 1999.
[9] N. Pulsone and C. Rader, "Adaptive beamformer orthogonal rejection test," *IEEE Trans. Signal Process.*, vol. 49, no. 3, pp. 521–529, Mar. 2001.
[10] G. A. Fabrizio, A. Farina, and M. D. Turley, "Spatial adaptive subspace detection in OTH radar," *IEEE Trans. Aerosp. Electron. Syst.*, vol. 39, no. 4, pp. 1407–1427, Oct. 2003.
[11] F. Bandiera, O. Besson, and G. Ricci, "An ABORT-like detector with improved mismatched signals rejection capabilities," *IEEE Trans. Signal Process.*, vol. 56, no. 1, pp. 14–25, Jan. 2008.
[12] A. De Maio, "Rao test for adaptive detection in Gaussian interference with unknown covariance matrix," *IEEE Trans. Signal Process.*, vol. 55, no. 7, pp. 3577–3584, Jul. 2007.

[13] S. Z. Kalson, "An adaptive arraydetector with mismatched signal rejection," *IEEE Trans. Aerosp. Electron. Syst.*, vol. 28, no. 1, pp. 195–207, Jan. 1992.
[14] S. Bose and A. O. Steinhardt, "A maximal invariant framework for adaptive detection with structured and unstructured covariance matrices," *IEEE Trans. Signal Process.*, vol. 43, no. 9, pp. 2164–2175, Sep. 1995.
[15] D. Ramirez, J. Via, I. Santamaria, and L. Scharf, "Locally most powerful invariant tests for correlation and sphericity of Gaussian vectors," *IEEE Trans. Inf. Theory*, vol. 59, no. 4, pp. 2128–2141, Apr. 2013.
[16] E. Conte, A. De Maio, and C. Galdi, "CFAR detection of multidimensional signals: An invariant approach," *IEEE Trans. Signal Process.*, vol. 51, no. 1, pp. 142–151, Jan. 2003.
[17] A. De Maio, "Generalized CFAR property and UMP invariance for adaptive signal detection," *IEEE Trans. Signal Process.*, vol. 61, no. 8, pp. 2104–2115, Apr. 2013.
[18] A. Coluccia, A. Fascista, and G. Ricci, "CFAR feature plane: A. novel framework for the analysis and design of radar detectors," *IEEE Trans. Signal Process.*, vol. 68, pp. 3903–3916, 2020.
[19] A. De Maio, "Invariance theory for adaptive radar detection in heterogeneous environment," *IEEE Signal Process. Lett.*, vol. 26, no. 7, pp. 996–1000, Jul. 2019.
[20] M. Tang, Y. Rong, A. De Maio, C. Chen, and J. Zhou, "Adaptive radar detection in Gaussian disturbance with structured covariance matrix via invariance theory," *IEEE Trans. Signal Process.*, vol. 67, no. 21, pp. 5671–5685, Nov. 2019.
[21] Y. Rong, A. Aubry, A. De Maio, and M. Tang, "Adaptive radar detection in low-rank heterogeneous clutter via invariance theory," *IEEE Trans. Signal Process.*, vol. 69, pp. 1492–1506, 2021.
[22] F. Bandiera, D. Orlando, and G. Ricci, *Advanced Radar Detection Schemes Under Mismatched Signal Models* (Synthesis Lectures on Signal Processing Series), vol. 8. San Rafael, CA, USA: Morgan & Claypool Publishers, 2009.
[23] A. Coluccia, G. Ricci, and O. Besson, "Design of robust radar detectors through random perturbation of the target signature," *IEEE Trans. Signal Process.*, vol. 67, no. 19, pp. 5118–5129, Oct. 2019.
[24] A. Coluccia, A. Fascista, and G. Ricci, "A k-nearest neighbors approach to the design of radar detectors," *Signal Process.*, vol. 174, Sep. 2020, Art. no. 107609.
[25] A. Coluccia, A. Fascista, and G. Ricci, "A KNN-based radar detector for coherent targets in non-Gaussian noise," *IEEE Signal Process. Lett.*, vol. 28, pp. 778–782, 2021.
[26] U. Zsolt, L. Lasdon, J. Plummer, F. Glover, J. Kelly, and R. Marti, "Scatter search and local NLP solvers: A multistart framework for global optimization," *INFORMS J. Comput.*, vol. 19, no. 3, pp. 328–340, Jul. 2007.
[27] C. Audet and J. E. Dennis Jr, "Analysis of generalized pattern searches," *SIAM J. Optim.*, vol. 13, no. 3, pp. 889–903, Jan. 2002.
[28] T. G. Kolda, R. M. Lewis, and V. Torczon, "Optimization by direct search: New perspectives on some classical and modern methods," *SIAM Rev.*, vol. 45, no. 3, pp. 385–482, Jan. 2003.
[29] D. E. Goldberg, *Genetic Algorithms in Search, Optimization and Machine Learning*, Reading, MA, USA: Addison-Wesley Longman Publishing Co., Oct. 1989.
[30] E. J. Kelly and K. Forsythe, "Adaptive detection and parameter estimation for multidimensional signal models," Lincoln Laboratory, MIT, Lexington, MA, Tech. Rep. 848, Apr. 1989.
[31] E. J. Kelly, "Adaptive detection in non-stationary interference-part III," Lincoln Laboratory, MIT, MA, Tech. Rep. 761, Aug. 1987.
[32] C. D. Richmond, "Performance of the adaptive sidelobe blanker detection algorithm in homogeneous environments," *IEEE Trans. Signal Process.*, vol. 48, no. 5, pp. 1235–1247, May 2000.
[33] J. B. Billingsley, A. Farina, F. Gini, M. V. Greco, and L. Verrazzani, "Statistical analyses of measured radar ground clutter data," *IEEE Trans. Aerosp. Electron. Syst.*, vol. 35, no. 2, pp. 579–593, Apr. 1999.
[34] M. Greco, F. Gini, A. Farina, and J. B. Billingsley, "Validation of windblown radar ground clutter spectral shape," *IEEE Trans. Aerosp. Electron. Syst.*, vol. 37, no. 2, pp. 538–548, Apr. 2001.
[35] A. De Maio and D. Orlando, "An invariant approach to adaptive radar detection under covariance persymmetry," *IEEE Trans. Signal Process.*, vol. 63, no. 5, pp. 1297–1309, Mar. 2015.
[36] D. Ciuonzo, D. Orlando, and L. Pallotta, "On the maximal invariant statistic for adaptive radar detection in partially homogeneous disturbance with persymmetric covariance," *IEEE Signal Process. Lett.*, vol. 23, no. 12, pp. 1830–1834, Dec. 2016.
[37] M. Tang, Y. Rong, X. R. Li, and J. Zhou, "Invariance theory for adaptive detection in non-Gaussian clutter," *IEEE Trans. Signal Process.*, vol. 68, pp. 2045–2060, 2020.
[38] M. Abramowitz and I. Stegun, *Handbook of Mathematical Functions With Formulas, Graphs, and Mathematical Tables*, vol. 55. Washington, D.C., USA: US Government Printing Office, 1972.
[39] I. S. Gradshteyn and I. M. Ryzhik, *Table of Integrals, Series, and Products*, San Diego, CA, USA: Academic Press, 2007.

Open Access provided by 'Università del Salento' within the CRUI CARE Agreement